

# Exploring the Interplay Between Ligand Derivatisation and Cation Type in the Assembly of Hybrid Polyoxometalate Mn-Andersons

Mali H. Rosnes, Chiara Musumeci, Carine Yvon, Andrew Macdonell, Chullikkattil P. Pradeep, Camillo Sartorio, De-Liang Long, Bruno Pignataro,\* and Leroy Cronin\*

**H**erein a library of hybrid Mn-Anderson polyoxometalates anions are presented: **1**,  $[(\text{MnMo}_6\text{O}_{18})((\text{OCH}_2)_3\text{-C-(CH}_2)_7\text{CHCH}_2)_2]^{3-}$ ; compound **2**,  $[(\text{MnMo}_6\text{O}_{18})((\text{OCH}_2)_3\text{-C-NHCH}_2\text{C}_{16}\text{H}_9)_2]^{3-}$ ; compound **3**,  $[(\text{MnMo}_6\text{O}_{18})((\text{OCH}_2)_3\text{-C-(CH}_2)_7\text{CHCH}_2)_1((\text{OCH}_2)_3\text{-C-NHCH}_2\text{C}_{16}\text{H}_9)_1]^{3-}$ ; compound **4**,  $[(\text{MnMo}_6\text{O}_{18})((\text{OCH}_2)_3\text{-NHC(O)CH}_2\text{CHCH}_2)_2]^{3-}$  and compounds **5–9**,  $[(\text{MnMo}_6\text{O}_{18})((\text{OCH}_2)_3\text{-NHC(O)(CH}_2)_x\text{CH}_3)_2]$ , where  $x = 4, 10, 12, 14,$  and  $18$  respectively. The compounds resulting from the cation exchange of the anions **1–9** to give TBA (**a**) and DMDOA (**b**) salts, and additionally for compounds **1, 2** and **3**, tetraphenylphosphonium ( $\text{PPh}_4$ ) (**c**) salts, are explored at the air/ water interface using scanning force microscopy, showing a range of architectures including hexagonal structures, nanofibers and other supramolecular forms. Additionally the solid-state structures for compounds **1c, 2c, 4a, 6a, 9a**, are presented for the first time and these investigations demonstrate the delicate interplay between the structure of the covalently derivatised hybrid organo-clusters as well as the ion-exchange cation types.

## 1. Introduction

Polyoxometalates (POMs) are molecular metal oxides built from metalates of Mo, W or V, sharing oxygen in either an edge- or corner- sharing manner.<sup>[1]</sup> They are a well-studied

class of materials associated with a wide variety of desirable properties, having shown to be highly redox, catalytically and biologically active, as well as showing potential as dielectric materials and devices.<sup>[2]</sup> In the Anderson structure, the addendum atom M is either  $\text{Mo}^{6+}$  or  $\text{W}^{6+}$ , where six  $\{\text{MO}_6\}$

Dr. M. H. Rosnes,<sup>[+]</sup> C. Yvon, A. Macdonell,  
Dr. C. P. Pradeep,<sup>[++]</sup> Dr. D.-L. Long, Prof. L. Cronin  
WestCHEM, School of Chemistry  
University of Glasgow  
University Avenue  
Glasgow, G12 8QQ, UK  
E-mail: Lee.Cronin@glasgow.ac.uk  
C. Musumeci,<sup>[+], [+++]</sup>  
Superlab-Consorzio  
Catania Ricerche  
Stradale Primosole 50, 95121 Catania, Italy

Dr. C. Sartorio, Prof. B. Pignataro  
Dipartimento di Fisica e Chimica  
Università di Palermo  
Viale delle Scienze  
Parco D'Orleans II, 90128 Palermo, Italy  
E-mail: bruno.pignataro@unipa.it



<sup>[+]</sup>These authors contributed equally to this work.

<sup>[++]</sup>Present Address: School of Basic Sciences, Indian Institute of Technology Mandi, Mandi 175 001, Himachal Pradesh, India

<sup>[+++]</sup>Present address: Nanochemistry Laboratory, ISIS, Université de Strasbourg, 8 allée Gaspard Monge, 67000 Strasbourg, France

DOI: 10.1002/sml.201202510

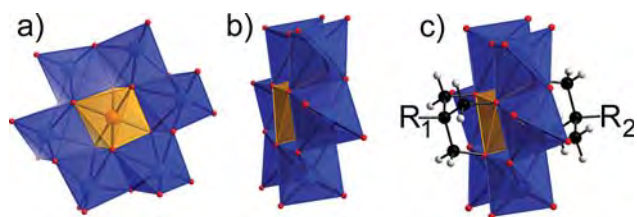


**Figure 1.** a) Top and b) side view of the Mn-Anderson cluster, with Mn in orange, Mo in blue and O in red. The oxygen atoms bridging the central Mn heteroatom, which can be replaced by oxygen atoms from organic ligands (i.e. methoxy ligands) are visible as the corners of the orange polyhedra, where it can be seen how the organic molecules are connected to the Mn-Anderson core (c).  $R_1$  and  $R_2$  are usually, but not always, equivalent.

edge sharing octahedra surround an edge-sharing central heteroatom, providing a central octahedral environment, as seen in **Figure 1a,b**.<sup>[3]</sup> Two ligands can be covalently attached to the “disk”-like cluster, one on each side, typically with  $Mn^{3+}$  as the central heteroatom, giving a range of organic-inorganic hybrids connected by covalent bonds.<sup>[4]</sup> A number of symmetric hybrid organic-inorganic Mn-Anderson compounds, where  $R_1$  equals  $R_2$ , have been reported,<sup>[5]</sup> but examples where  $R_1$  is not equal to  $R_2$  have also been reported (see **Figure 1c**), resulting in so-called asymmetrically or unsymmetrically substituted Mn-Anderson compounds.<sup>[6]</sup>

In our attempt to explore the self-assembly of hybrid Mn-Anderson compounds at the air/water interface we have previously employed the Langmuir-Blodgett (LB) technique, which resulted in well-defined nanostructures, as observed by scanning force microscopy (SFM) imaging of the films when transferred onto solid substrates. A study of three Mn-Anderson compounds revealed their self-assembly behavior and suggested that this behavior may be dependent on the properties of the organic moieties both grafted to the POM, and also employed within the counter cations.<sup>[6a]</sup> Similar results from drop-casting deposition of hybrid POMs indicate that it is possible to induce the formation of self-organized architectures with a wide variety of shapes and dimensionalities by changing certain chemical parameters and/or dynamic conditions.<sup>[7]</sup> Given these initial observations, we thought that it is important to expand and unify our work to explore our initial hypothesis, and also to expand the library of POM-hybrids and their investigation at interfaces, yet to accomplish this would require a full library of POMs that can be systematically varied and compared.

Herein, we present a library of Mn-Anderson compounds with varied, but structurally related, organic ligands and cations, along with detailed syntheses and characterization, including X-ray crystallographic data. We also investigate how the nature of the organic ligands and cations directs, and contributes to the overall self-assembly behavior of the compounds on surfaces. In order to have fine control over the employed experimental parameters (surface pressure, temperature etc.) along with a high resolution of the structures, we specifically use the LB technique to transfer the POM-based architectures onto flat hydrophilic surfaces (mica or hydroxylated silicon), and dynamic SFM both in attractive and

repulsive regime,<sup>[8]</sup> for imaging. In total, nine Mn-Anderson compounds are investigated and reported here: compound **1**,  $[(MnMo_6O_{18})((OCH_2)_3C-(CH_2)_7CHCH_2)_2]^{3-}$ ; compound **2**,  $[(MnMo_6O_{18})((OCH_2)_3C-NHCH_2C_{16}H_9)_2]^{3-}$ ; compound **3**,  $[(MnMo_6O_{18})((OCH_2)_3C-(CH_2)_7CHCH_2)_1((OCH_2)_3C-NHCH_2C_{16}H_9)_1]^{3-}$ ; compound **4**,  $[(MnMo_6O_{18})((OCH_2)_3C-NHC(O)CH_2CHCH_2)_2]^{3-}$  and compounds **5-9**,  $[(MnMo_6O_{18})((OCH_2)_3C-NHC(O)(CH_2)_xCH_3)_2]$ , where  $x = 4, 10, 12, 14$  and  $18$  respectively. The cations employed were tetrabutylammonium (TBA) (**a**), dimethyldioctadecylammonium (DMDOA) (**b**), and, for compounds **1**, **2** and **3**, tetraphenylphosphonium (PPh<sub>4</sub>) (**c**), see **Table 1** for an overview of the compounds. The synthesis and surface analysis of compounds **1a**,<sup>[6a]</sup> **1b**,<sup>[2c]</sup> **2a**,<sup>[5c,6a]</sup> and **3a**<sup>[6a]</sup> have been reported previously, and are only included here for comparison. The synthesis of compounds **5a**,<sup>[5b]</sup> **7a**,<sup>[5c]</sup> **8a**<sup>[5b]</sup> and **8b**<sup>[5b]</sup> have been reported previously, but here we describe their self-assembly on surfaces as well as compare and contrast some of the crystal structures of these compounds allowing us to present a general set of conclusions and that will be important for the development of the area of polyoxometalate-hybrid cluster compounds.

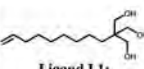
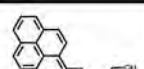
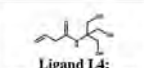
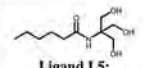
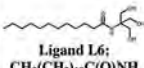
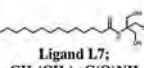
## 2. Results

The hybrid Mn-Anderson compounds were all synthesized using literature procedures in which the ligands react with  $\alpha$ - $[Mo_8O_{26}(TBA)_4]^{9-}$  and  $Mn(OAc)_3 \cdot 2H_2O$  in acetonitrile,<sup>[4,5c]</sup> with the exception of compound **3a**<sup>[6]</sup> (for experimental details see the Supporting Information (SI)). Crystallographic and surface studies of these compounds are reported below.

### 2.1. Crystallography

The crystal structures of compounds **1a**,<sup>[6a]</sup> **2a**,<sup>[5c]</sup> **3a**,<sup>[6a]</sup> **5a**,<sup>[5b]</sup> **7a**<sup>[5c]</sup> and **8a**<sup>[5b]</sup> have been previously reported, while the crystal structures for compounds **4a**, **6a**, **9a**, **1c** and **2c** are reported here for the first time, however we present a general structural analysis that compares and contrasts both this new, and our previous, work. What is really interesting is that, despite the fact the clusters are appended with long carbon chains, the atoms in these chains could be resolved in the structures of compounds **1c**, **2c**, **4a** and **9a**, with only the carbon chains of **6a** not being fully resolvable. A table summarizing the new crystallographic data presented in this paper is presented in the SI (Table S1) and it is interesting to note that in the structural data obtained for almost all the compounds, in particular **1a**, **2a** and **3a**, the most prominent interaction is the  $C-H \cdots O = Mo$  hydrogen bonded interaction. This is perhaps responsible for anchoring the long carbon chains in one particular conformation allowing them to be resolved crystallographically. For compound **1a** these  $C-H \cdots O = Mo$  hydrogen bonds are particularly evident between the terminal groups of the  $C_9$ -chains and the metal oxides. The crystal packing of compound **1c** is similar to **1a** in that the carbon chains align to maximise the  $Mo = O \cdots HC$  hydrogen bond interaction, as seen in **Figure 2**. (Solvent

**Table 1.** An overview of the ligands, cations and compounds is presented. For compounds that have been reported elsewhere the reference is given. Their lengths are inferred using the crystallographic data. All the values are given in nanometers and are just for comparison.

		The Mn-Anderson compounds [MnMo <sub>6</sub> O <sub>18</sub> ((OCH <sub>2</sub> ) <sub>3</sub> -C-R <sub>1</sub> )((OCH <sub>2</sub> ) <sub>2</sub> -C-R <sub>2</sub> )] <sup>+</sup>			Diameter (D) and Length (L) (in nm) (from X-ray data)
Ligand	Cation	TBA 	DMDOA 	PPh <sub>4</sub> 	
			(N(C <sub>4</sub> H <sub>9</sub> ) <sub>4</sub> )	(N(CH <sub>3</sub> ) <sub>2</sub> (C <sub>18</sub> H <sub>37</sub> ) <sub>2</sub> )	(P(C <sub>6</sub> H <sub>5</sub> ) <sub>4</sub> )
Ligand L1; CH <sub>2</sub> CH(CH <sub>2</sub> ) <sub>7</sub> - C(CH <sub>2</sub> OH) <sub>3</sub> 		1a <sup>[6a]</sup>	1b <sup>[2c]</sup>	1c	D = 0.9 L = 2.45
Ligand L2; C <sub>16</sub> H <sub>9</sub> CH <sub>2</sub> NH- C(CH <sub>2</sub> OH) <sub>3</sub> 		2a <sup>[3c/5a]</sup>	2b	2c	D = 0.9 L = 2.55
Ligand L1 & L2 together; CH <sub>2</sub> CH <sub>2</sub> (CH <sub>2</sub> ) <sub>7</sub> - (-C(CH <sub>2</sub> OH) <sub>3</sub> )(R <sub>1</sub> ) & C <sub>16</sub> H <sub>9</sub> CH <sub>2</sub> NH (-C(CH <sub>2</sub> OH) <sub>3</sub> )(R <sub>2</sub> )		3a <sup>[6a]</sup>	3b	3c	D = 0.9 L = 2.45
Ligand L4; CH <sub>2</sub> CHCH <sub>2</sub> C(O)NH- C(CH <sub>2</sub> OH) <sub>3</sub> 		4a	4b		D = 0.9 L = 2.1
Ligand L5; CH <sub>3</sub> (CH <sub>2</sub> ) <sub>4</sub> C(O)NH (-C(CH <sub>2</sub> OH) <sub>3</sub> ) 		5a <sup>[5b]</sup>	5b		D = 0.9 L = 2.6
Ligand L6; CH <sub>3</sub> (CH <sub>2</sub> ) <sub>10</sub> C(O)NH (-C(CH <sub>2</sub> OH) <sub>3</sub> ) 		6a	6b		D = 0.9 L = 3.9
Ligand L7; CH <sub>3</sub> (CH <sub>2</sub> ) <sub>12</sub> C(O)NH (-C(CH <sub>2</sub> OH) <sub>3</sub> ) 		7a <sup>[5d]</sup>	7b		D = 0.9 L = 4.5
Ligand L8; CH <sub>3</sub> (CH <sub>2</sub> ) <sub>14</sub> C(O)NH (-C(CH <sub>2</sub> OH) <sub>3</sub> ) 		8a <sup>[5b]</sup>	8b <sup>[5b]</sup>		D = 0.9 L = 5.1
Ligand L9; CH <sub>3</sub> (CH <sub>2</sub> ) <sub>16</sub> C(O)NH (-C(CH <sub>2</sub> OH) <sub>3</sub> ) 		9a	9b		D = 0.9 L = 6.1

molecules, cations and disorder are omitted for clarity in all the crystallography presentations, and the colour scheme is Mo, blue; O, red; C, black; N, cyan; H, white.) The smallest Mo = O...O = Mo distance observed for **1c** is about 3.8 Å. The shortest distance between the carbon chains, C...C, best seen in Figure 2b, is 3.8 Å indicating a range of short-range hydrophobic interactions. The PPh<sub>4</sub> cations are omitted for clarity, but perpendicular CH...π interactions at 2.65(2) Å are observed.<sup>[10]</sup> For both compounds **1a** and **2a** the hydrogen bonding and van der Waals interactions are the only interactions observed. For compound **3a** however, CH...π interactions between the alkyl chains and pyrene ligands across molecules are observed, in addition to the C-H...O = Mo hydrogen bond, resulting in a highly ordered pattern.

Compound **2c** contains the same bis-pyrene Anderson unit as found in **2a**, but we purposely swapped the TBA counter ions to PPh<sub>4</sub> in an effort to engineer π-π interactions since in **2a** CH...O = Mo hydrogen bonded interactions dominated with no π-π interactions. The packing of **2c** is shown in Figure 2e-f which indeed shows that when the cation is changed to PPh<sub>4</sub>, strong interactions between the pyrene moieties of one metal oxide with a pyrene moiety each on two adjacent metal oxides are evident. The shortest distance between the pyrene moieties is 3.46(3) Å, which corresponds well to the predicted distance for such π-π interactions, and the pyrene units are slightly offset to each other, as expected.<sup>[10]</sup> The chains of π-π-linked clusters are supported by perpendicular metal oxides, through CH...O = Mo hydrogen bonding, of around 2.5-2.6 Å in distance, reported to normally be in the range 1.8 to 2.5 Å.<sup>[11]</sup>

In compound **4a** it can be seen that the C<sub>4</sub>-carbon chain of one metal oxide is associated towards the C<sub>4</sub>-carbon chain of the adjacent metal oxide, resulting in a 'wave'-like structure, see Figure 3, with the distance between alkyl chains of around 2.3 Å, indicating hydrophobic interactions. It can also be seen how the metal oxides are aligned next to each other, but with a separation of around 15 Å.

In compound **6a**, the C<sub>10</sub> carbon chains are not fully resolved and the organic moieties in adjacent molecules are aligned towards a central 'cavity' maximising the hydrophobic interactions, see Figure 4. In contrast compound **7a** crystallises well-ordered in orange block shaped crystals in a monoclinic crystal system. The positions of all the atoms have been crystallographically determined for compound **7a**. This leads to a fascinating and aesthetically pleasing pattern, where the alkyl chains are aligned towards the same centre as six other metal oxides in the plane. The CH...HC distance between the alkyl chains is about 3 Å, indicating hydrophobic interactions, see Figure 4 for details (although the structure has previously published a representation or discussion of the packing has not before been presented).<sup>[5c]</sup>

Compound **9a** crystallises as orange block shaped crystals in a triclinic crystal system, and the positions of all the carbon atoms have been crystallographically determined, which is quite amazing given that the chains are 19 carbon atoms long. The hydrogen atoms are not depicted. However, as indicated by both compounds **6a** and **8a**, the alkyl chains from the metal oxides are arranged towards the same centre, resulting in hydrophobic 'channels', see Figure 4. The distances between

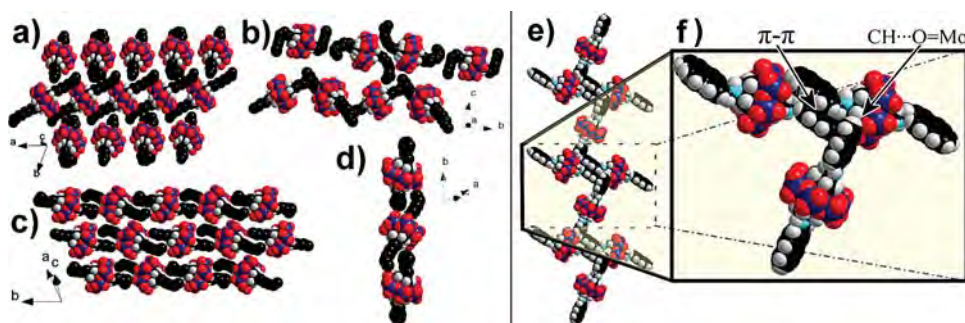


**Figure 2.** Packing system for compound **1c** is shown on the left (a-d). The protons are omitted, but it can be seen that the alkyl-chains are positioned to increase the potential of Mo = O...HC hydrogen bond interactions. Packing system for compound **2c** is shown on the right (e-f). In between the ‘horizontal chains’ linked by  $\pi$ - $\pi$  interactions, ‘vertical’ compounds are positioned to maximise the CH...O = Mo between the pyrene moieties and the metal oxide core.

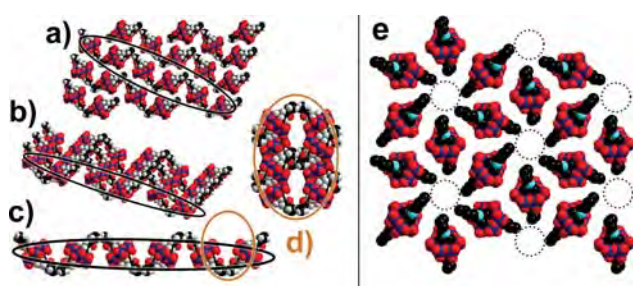


**Figure 3.** Packing system for compound **4a** is shown on the left (a-d). In (b) a view of the highlighted area from a) is shown from the side, but still showing the layer, whilst in (c) the side on view of the layer is shown. In (d) the side-on view when two layers are on top of each other is shown. Packing system of compound **6a** is shown on the right (e), viewed along the crystallographic *c*-axis.

the moieties are difficult to determine as the hydrogen atoms are not present, however, the smallest C...C distance is about 3.96–4.50 Å, so hydrophobic interactions are evident. Hydrogen bond interactions between the amide groups and adjacent terminal oxo groups are also present, with the NH...O = Mo distance being about 2.00–2.40 Å. Finally, the closest C...O = Mo distance is about 3.07 Å, indicating C–H...O = Mo hydrogen bonds.

## 2.2. Self-Assembly at the Air/Water Interface

Compounds **1–9** were dissolved at concentrations of 2–5 mg/mL in a mixture of MeCN and CHCl<sub>3</sub>, with a volume ratio of 1:1 or 1:2. Details of the film preparation by LB, along with the respective isotherms are reported in the SI. Samples were deposited at surface pressures high enough to make the structures assemble as well-defined architectures (10–30 N/m). The LB layers deposited onto hydrophilic substrates were left to dry in air and

subsequently observed by dynamic SFM. Both dynamic non-contact (attractive regime)<sup>[8]</sup> and intermittent-contact modes were employed for the morphological characterization of the transferred films.

**Compounds 1–3:** The matrix comparing compounds **1–3** is presented in **Figure 5**. It can clearly be seen that the surface architecture is dependent on both the organic ligand and the organic cation employed. It is particularly interesting to observe how the architectures obtained from compound **1** change; as the TBA salt (**1a**)<sup>[6a]</sup> and the PPh<sub>4</sub> salt (**1c**) only undefined islands were seen, but by changing the cation to the DMDOA surfactant (**1b**), well defined hexagonal nanostructures were observed.<sup>[2c]</sup> Compounds **2b** and **3b** form more rounded, non-uniform, hexagon-like structures. Remarkably, the height (3.8 nm) and the smooth top-surface (0.2 nm RMS) of these structures is the same as that observed for **1b**. While well-arranged fibers were seen for compounds **2a** and **3a** with TBA cations,<sup>[6a]</sup> PPh<sub>4</sub> allows for the formation of compact layers. In particular, compound **2c** results in a 1

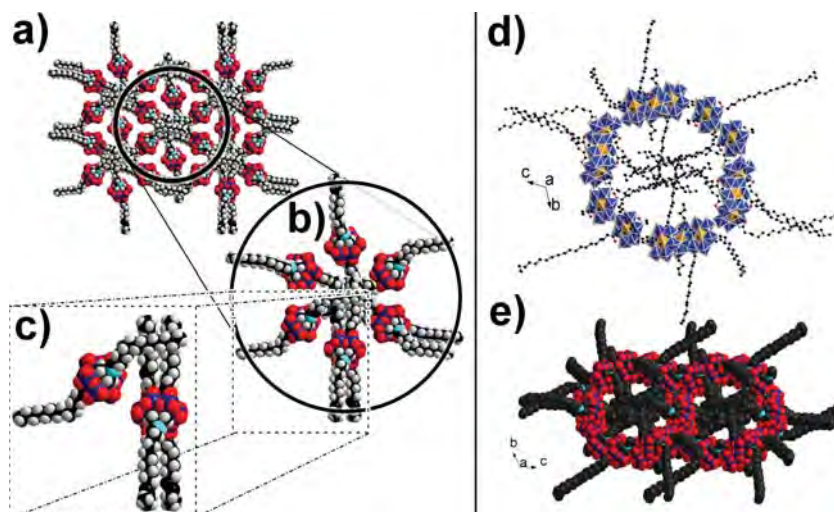


**Figure 4.** The crystal packing for compound **7a** is presented on the left, viewed along the crystallographic *x*-axis. The ‘flower’-like pattern is shown in (a), (b) is a magnification of the ‘alkyl’ center, and (c) shows how three of the Mn-Anderson compounds align in the system. The crystal packing for compound **9a** is displayed on the right. (d) is viewed along the crystallographic *a*-axis, whilst (e) is viewed from the opposite direction. The circular pattern is shown with the central ‘alkyl’ centre, or channels are evident.

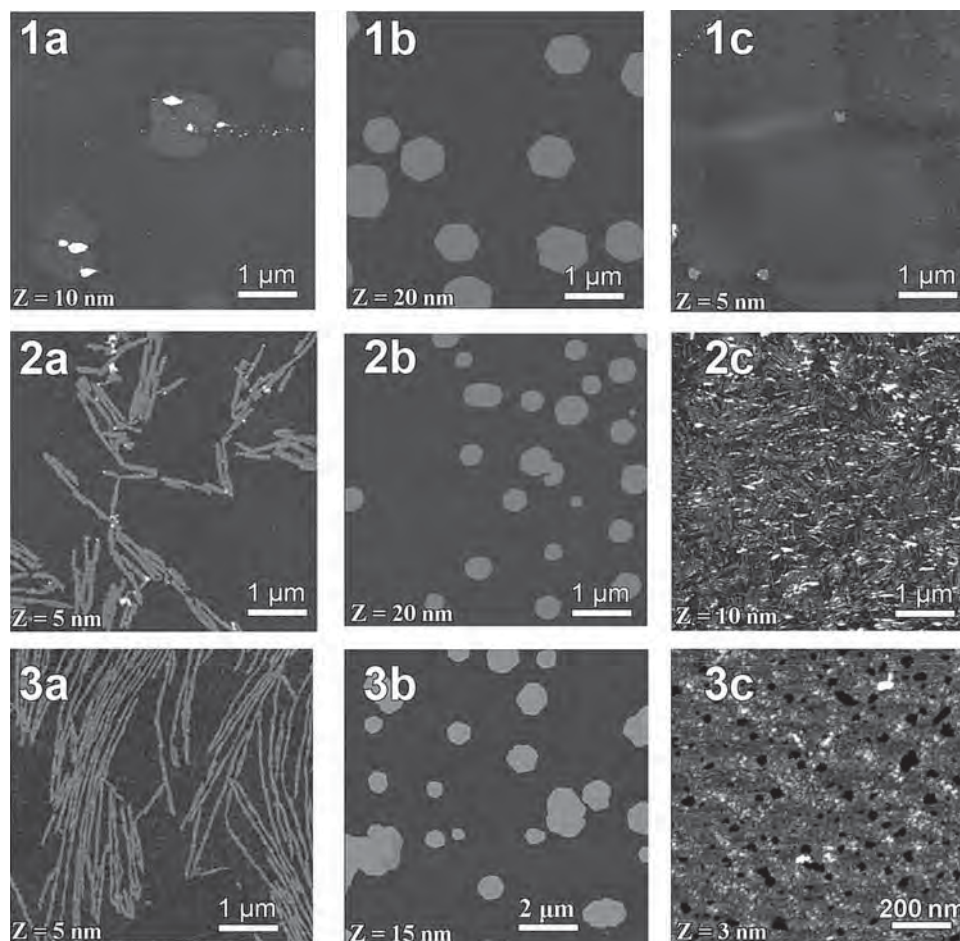


**Figure 5.** SFM results for compounds **1**, **2** and **3** with different cations. Moving down a specific column the influence of the organic ligands on the structural trends is evident. Likewise, moving along a row, the effect of the organic cations employed is also evident. In particular, the trend observed for the DMDOA compounds is apparent when comparing compounds **1b**, **2b** and **3b**. The fact that the vertical trends are more striking than the horizontal might indicate that the cations play a more significant role in directing the observed architectures, with the organic ligands playing more of a fine-tuning role.

nm thick layer, plus the appearance of individual nanorods of about 1–3 nm in diameter, whilst **3c** forms a compact layer, about 3 nm in thickness.

**Compounds 4–9:** For compounds **4–9** all the organic ligands are linked to the Mn-Anderson tris-stem *via* amide bonds, where the chain length steadily increases: C<sub>4</sub> (**4**), C<sub>6</sub> (**5**), C<sub>12</sub> (**6**), C<sub>14</sub> (**7**), C<sub>16</sub> (**8**) and C<sub>20</sub> (**9**). Compound **4** contains a terminal double bond, but is otherwise the same as the other compounds. These compounds are very similar in structure to compound **1**, save for the amide-linkage; however, their surface behavior is very different. Definite trends can be observed for both the length of the carbon chain and the nature of the cation. An overview of the obtained architectures is depicted in **Figure 6**.

The two compounds with shorter chain length (**4a** and **5a**) were likely partially soluble in the subphase, explaining why it was not possible to reach high pressure at the air/water interface (see isotherms in Figure S2 in the SI). As a result, only small aggregates randomly distributed over the solid substrate can be obtained for compound **4a**, whilst for compound **5a** a monolayer consisting of a low-density, liquid-like

phase of about 0.8 nm in height was obtained, correlating to the clusters lying more or less parallel to the substrate. More well-defined isotherm curves can be obtained for compounds **6a–9a**, due to their higher degree of hydrophobic character. These compounds assemble in ultrathin films which appear extremely compact, to the extent that it is quite difficult to distinguish isolated and defined nanostructures. Nevertheless, the anisotropic nature of molecular aggregates can be observed by the high-magnification images (see below in the Discussion section).

Anisotropic fibrillar assemblies are observed for all the DMDOA compounds (**4b–9b**). For compounds **4b** and **5b**, well-defined individual and evenly distributed straight, fibrous strands about 1 nm in height are observed. Similar structures, but with a decreased strand length and rigidity, can be observed for compounds **6b–9b**. This is consistent with a decreased limit area when the chain length is increased. In some cases, randomly distributed molecules are present in-between the strands, appearing as an ultrathin uppermost layer.

High resolution images of compound **8a** are reported in **Figure 7**, showing a very definite molecular alignment into an

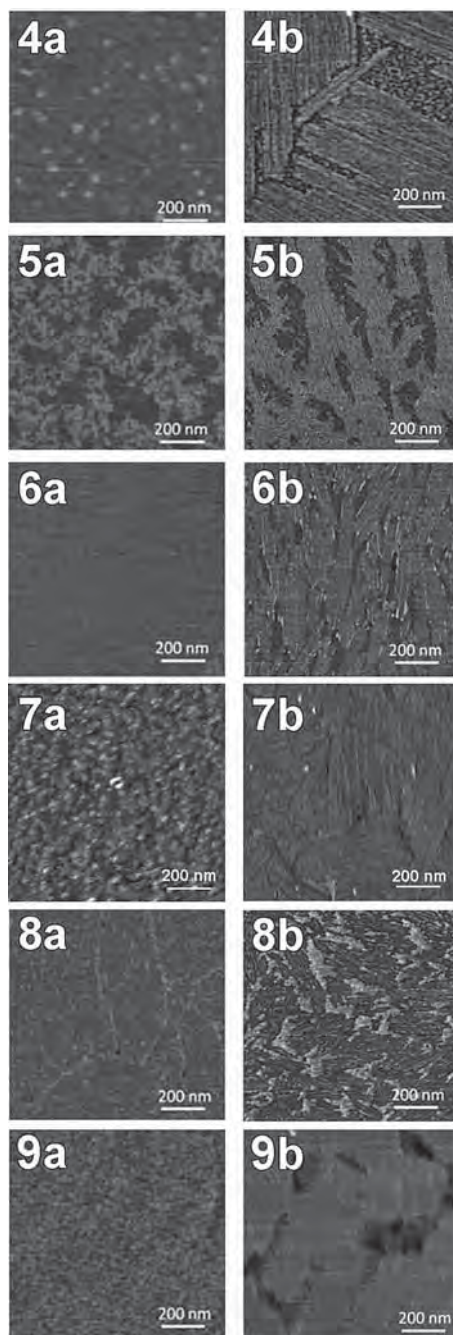


**Figure 6.** A presentation of the SFM height images of the LB films obtained for compounds **4a-9a** and **4b-9b**. The  $z_{\text{scale}}$  is 3 nm for all the images.

anisotropically textured film. The thickness of the film measured by section analysis is  $0.7 \pm 0.2$  nm, and is consistent with an arrangement where molecules lie with the POM clusters' axes parallel to the substrate. In both Figure 7a and the high magnification image in Figure 7b, different alignment directions are visible, indicating that the formation of these anisotropic structures is not due to the transfer process but is rather a result of the molecular self-assembly at the air/water interface. The general structure of the films of compounds **6a**,

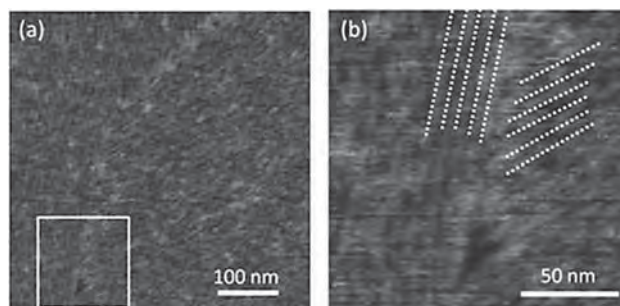


**Figure 7.** SFM height images showing the anisotropic nature of the thin film obtained for compound **8a** on mica. The average thickness of the layer is 0.7 nm. The image in (b) is a close-up of (a) within the marked square where the dotted lines highlight the almost straight molecular alignments. The lateral peak-to-peak distance measured by section analysis is about 6 nm. The  $z_{\text{scale}}$  is 3 nm.

**7a** and **9a** are very similar to that obtained for compound **8a**, but the compactness of the anisotropic texture diminishes with increasing molecular chain length. While it is difficult to estimate the periodicity of the anisotropic structures of compound **6a** and **7a**, for compound **8a** it can be measured to be about 6 nm, while compound **9a** shows a lateral fiber-to-fiber distance of about 20 nm. Accordingly, the limit areas from the isotherm plots (see the SI) of compounds **6a**, **7a**, **8a** and **9a** show increasing values respectively of 110, 140, 160 and  $175 \text{ \AA}^2$ .

### 3. Discussion

The investigation of this library of Mn-Anderson compounds has provided a wealth of synthetic and crystallographic data, elemental characterization, and information on the compounds' surface behavior. From this, we have attempted to deduce trends in the compounds' behavior, based on the nature of the metal oxide, organic ligand and cation building-blocks employed. We envisage that it should be possible to exploit the observed trends to assemble a tool-box of systems suitable for self-assembly in a predefined manner. Thus, in an attempt to predict and understand the self-assembly of these compounds, we looked at the trends in their crystallographic structures, and their behavior at hydrophilic interfaces. Crystallographic data were only obtained for the compounds with TBA and  $\text{PPh}_4$  as the organic counter cation, since we were unable to grow single crystals of good enough quality for the compounds with DMDOA. (To our knowledge only one POM with DMDOA as the cation has been successfully characterized by X-ray crystallography.<sup>[12]</sup>) However, by comparing the trends observed for the various ligands and cations, conclusions can still be drawn regarding the DMDOA compounds. To discuss the results, we first looked at the data for compounds **1-3** and compounds **4-9** separately, and then compared all the compounds in an attempt to find trends in behavior related to the nature of both the organic ligands and cations employed.

**Compounds 1-3:** Looking at the crystallographic data for compounds **1a-3a** there are little to no  $\pi \cdots \pi$  interactions,

despite expectations that the pyrene moieties would introduce such interactions. However, hydrogen bonding from the ligands to the terminal oxo groups in the metal oxide core is evident. In the surface organization it can be seen that compound **3a** gives fibers with higher aspect ratio compared to those of **2a** (which has wider but shorter fibers), and this is likely to arise from the enhanced  $\pi\cdots\pi$  interaction possibilities in compound **2a**.<sup>[6a]</sup> It is important to note that the interactions most dominant from the crystallographic data might not be as important for the surface architectures, as a hydrophilic sub-phase and substrate were employed, which can affect the nature of the interactions.

For compounds **1b-3b**, no crystallographic data are available, but the architectures obtained from the three compounds seem more closely related, compared to those observed for compounds **1a-3a**. This indicates that it is principally the nature of the cation which controls the self-assembly processes in these instances, where the larger size of the DMDOA cations keeps the Mn-Anderson anions further apart, reducing the interaction between them. The formation of the hexagonal aggregates has already been reported for compound **1b**,<sup>[2c]</sup> and it was found that the hexagonal aggregates arise from the reorganization of a liquid-condensed phase and the instauration of van der Waals interactions among the alkyl chains. Compounds **2b** and **3b** have the same cation to anion stoichiometry as compound **1b**, where there are three cations for each anion, and hexagonal-like structures were expected. The interactions of the aliphatic chains are found to be one of the main factors for this peculiar molecular packing with the DMDOA cation, and the presence of long alkyl moieties on both sides of the POM cluster (**1b**) allows the formation of more ordered and regular architectures.

For compounds **1c-3c** it is again only **2** and **3** that form defined architectures, so although the  $\text{PPh}_4$  cation introduces the possibility for  $\pi\cdots\pi$  interactions, compound **1c** does not form any defined architectures. The reason for this is unclear, but might be due to the fact that there is no moiety on the organic ligand of the Mn-Anderson compound, meaning only  $\pi\cdots\pi$  interactions between cations themselves can occur, which may not be sufficient for lateral packing. The fact that compounds **2c** and **3c** form highly congested surface patterns might be due to the high concentration of aromatic moieties, allowing for  $\pi\cdots\pi$  interactions. Interestingly, by employing a mixture of TBA and  $\text{PPh}_4$  cations (i.e. when the cation exchange reaction had not gone to completion) different features are observed for these compounds. (Figure S4 and S5 and discussion under section 8 the SI). Although further specific studies are needed, this suggests that the variation of the TBA/  $\text{PPh}_4$  ratio might be a very interesting route to modulate the self-assembly, along with the mechanical behavior of POM-based fiber-like structures.

**Compounds 4a-9a:** As mentioned previously compound **4a** does not result in well-defined transferred films, and nor does **5a**, whilst compounds **6a-9a** assemble into compact LB films, probably due to stabilization by the longer hydrophobic tails. Moreover, the longer the organic ligands the larger the distance between fibers and the larger the limit area in the Langmuir isotherms, which suggests that the organic tails act

as spacers between aligned POM clusters. The small height of the architectures suggests that the organic ligands are aligned almost parallel to the substrate plane, hence these structures are not likely to be molecular dimensional mismatch-induced ripple phases at surfaces.<sup>[13]</sup> The nature of the nano-scale periodicity and the random orientation of the anisotropic domains strongly indicate that they are also not the result of the LB transfer.<sup>[14]</sup>

**Compounds 4b-9b:** It has been shown that when DMDOA·Br films are fabricated in the presence of Anderson-type clusters ( $\{\text{SbW}_6\}$  and  $\{\text{MnW}_6\}$ ) in the sub-phase, the isotherms exhibit a decrease in the molecular area, and an increase in the surface pressure compared to when the subphase is pure water,<sup>[15]</sup> suggesting a closer packing when the repulsion among the DMDOA cations is minimized by the negative charges of the Anderson anions. For the DMDOA Mn-Anderson compounds presented here, the isotherms exhibit an increase in the mean molecular area compared to pure DMDOA·Br (see the SI), due to the organic ligands grafted onto the Mn-Anderson compounds. The aliphatic lateral chains on the ligands are likely to keep the clusters at the air/water interface, allowing them to take part in the formation of the monolayer. In contrast to the **1b-3b** series, the **4b-9b** compounds assemble in strands, which change in terms of rigidity and orientation. In particular, long and straight fibers are obtained for compound **4b** having the shortest ligand, while the least ordered strands are observed for compound **9b**, the one with the longest organic ligand.

The results obtained from compounds **4-9** show that, by properly combining amide-derived H-bonds and alkyl chains, it is possible to obtain anisotropic structures with tunable rigidity and orientation. As above, for compounds **4a-9a**, data are not in agreement with ripple phases or transfer instability effects.

**Comparison of All Compounds:** One of the most surprising results of this study is the unusual behavior of compound **1** compared to compounds **4-9**, considering the similarity in the organic ligands employed. Compared to compounds **5-9**, compound **1** is the only one with terminal double bonds, and it could be argued that this causes the difference in behavior. However, compound **4** also contains terminal double bonds, yet its surface architecture is unmistakably similar to that of compound **5**, ruling out this hypothesis. The more likely explanation is that the geometry of the atom next to the tertiary carbon atom of the tris-moiety (the atom in the fourth position away from the Mn-center) results in the observed differences. For compound **1**, this atom is a  $\text{sp}^3$  hybridized tetrahedral carbon atom allowing free rotation, (compounds **2** and **3** also have free rotation in this position), whilst for compounds **4-9** a nitrogen atom involved in an amide bond occupies the same position, introducing steric hindrance. As well as the steric hindrance there is one other vital difference between the compounds; only the amide moieties can form hydrogen bonds between alkyl ligands. It is unclear exactly how this restriction of rotation and possibility for hydrogen bonding between the ligands can alter the surface architectures to such an extent, and further investigations are needed.

## 4. Conclusion

In summary, we have synthesized and fully characterized eight organic ligands with tris-like moieties, by which they were linked to the Mn-Anderson core. Detailed synthetic procedures and extensive characterizations of both the organic ligands and their respective Mn-Anderson compounds are reported here. Cation exchange processes were also successfully carried out, and the products were carefully characterized using a wide range of analytical tools, with a particular focus on the crystallographic data for the TBA Mn-Anderson compounds, looking at the possible interactions within the structures.

Using SFM analysis, we have studied the presented library of Mn-Anderson compounds on solid substrates obtained by LB induced depositions, yielding a preliminary model for multifunctional POM-based systems self-assembled on surfaces. The investigation looked at how varying the organic ligand covalently bound to the Mn-Anderson cluster and the organic cations associated with it affected the self-assembly process at the air/water interface, with five notable patterns emerging. Firstly, the lengths of the alkyl chains in the ligands affect the surface architectures, evident in the directionality and uniformity of the observed architectures for compounds **4-9**. Secondly, the chemical nature of the organic cation (aromatic or aliphatic) and the length of the alkyl chains, affects the supramolecular structure, as can be seen by comparing the results obtained for the **a**, **b** and **c** forms of any compound. Thirdly, the geometry of the atom next to the tertiary carbon atom in the tris-moiety has a specific effect on the surface architectures, highlighted by the hexagonal nanostructures obtained for compound **1b** compared to compounds **4b-9b**, and supported by the fact that compounds **2a** and **3a**, with a freely rotating amine linkage, also form defined and individual architectures, while compounds **4a-9a** do not. Fourthly, the compounds with amide linkages are more likely to form intermolecular hydrogen bonds (between alkyl chains). Finally, the ratio of aromatic moieties to alkyl moieties present in both the ligands and cations affects the architectures, allowing both  $\pi\cdots\pi$  and hydrophobic interactions, as highlighted in the study of **2a** and **3a**, where the length, uniformity and directionality of the observed domains can be related to this ratio. The presence of alkyl chains favors a more linear orientation, while the presence of aromatic moieties favors the formation of more compact assemblies.

These five observations could prove to be useful for constructing an architectural toolbox for controlling self-assembly on surfaces, providing a means to conveniently change the surface structure by employing the correct combination of POM, organic ligand and cation, allowing the tuning of properties such as rigidity and molecular orientation. This is an important step towards the future rational design of 'soft-matter' architectures that incorporate metal oxides and may allow soft routes to functional devices, since knowledge of how the different moieties influence the overall architectures can be used to inform the synthesis of specifically designed multifunctional POM-organic hybrids.

## 5. Experimental Section

**Materials and Analysis:** Details for all the reagents and analytical tools used in the present study are provided in the SI.

**Precursor Synthesis:** (TBA)<sub>4</sub>[ $\alpha$ -Mo<sub>8</sub>O<sub>26</sub>] were prepared as described in reference [9].

**Typical Ligand Synthesis:** The organic ligands were all synthesized according to literature procedures. Except for **L1** and **L2**,<sup>[5e,6a]</sup> all the ligands were synthesized according to one general amide coupling procedure,<sup>[16]</sup> presented here with the synthesis of **L9**: To a solution of arachidic acid (2.28 g, 7.3 mmol) and *N*-methylmorpholine (0.9 mL, 8 mmol,  $\rho = 1.013 \text{ g mL}^{-1}$ ) in THF (10 mL) at 0 °C, ethylchloroformate (0.8 mL, 8.0 mmol,  $\rho = 1.1403 \text{ g mL}^{-1}$ ) was added dropwise and the reaction mixture was stirred at 0 °C for 30 min. The precipitate was filtered off and the filtrate was added to a pre-mixed (10 min) solution of tri-base (0.892 g, 7.3 mmol) and triethylamine (1.1 mL, 8.0 mmol,  $\rho = 0.7255 \text{ g mL}^{-1}$ ) in DMF (10 mL). The reaction mixture was kept stirring for ~50 min at room temperature, then the solvent was removed under vacuum, before the resulting precipitate was washed with water and dried to yield **L9** as a white powder. Yield: 66%.

**Typical Mn-Anderson Synthesis:** The TBA versions of the Mn-Anderson compounds were synthesized based on the standard literature procedure,<sup>[4]</sup> except for compound **3a**.<sup>[6]</sup> The standard procedure is presented here with the synthesis of compound **9a**, (TBA)<sub>3</sub>[MnMo<sub>6</sub>O<sub>18</sub>((OCH<sub>2</sub>)<sub>3</sub>C-NH-CO-(CH<sub>2</sub>)<sub>18</sub>-CH<sub>3</sub>)<sub>2</sub>]: (TBA)<sub>4</sub>[ $\alpha$ -Mo<sub>8</sub>O<sub>26</sub>] (1.50 g, 0.70 mmol), Mn(OAc)<sub>3</sub>·2H<sub>2</sub>O (0.28 g, 1.05 mmol) and **L9** (7.0 g, 2.41 mmol) were refluxed in MeCN (40 mL) for 16 hours. The orange reaction mixture was then cooled to room temperature and the precipitate was removed by centrifugation. The solution was set up for crystallization with diethyl ether diffusion. After about 1 week the product was collected as an orange crystalline material and dried. Yield: 75% based on Mo.

**Cation Exchange:** The cation exchange products with DMDOA and PPh<sub>4</sub> are all prepared from the TBA Mn-Anderson compounds. The DMDOA exchanges were based on a literature procedure.<sup>[5b]</sup> See the supporting information for details.

**Langmuir Blodgett deposition:** For the Langmuir-Blodgett deposition the compounds were dissolved at concentrations of 2–5 mg/mL in a mixture of MeCN and CHCl<sub>3</sub> with a volume ratio of 1:1 or 1:2. Drops of the above solutions were randomly spread over the aqueous sub-phase and the floating films were linearly compressed by two mobile barriers at a rate of 5 mm/min. The LB layers deposited onto mica, or hydroxylated silicon, were left to dry in air and subsequently observed by dynamic SFM.

**Dynamic Scanning Force Microscopy (SFM):** A Multimode Nanoscope IIIa, from Digital Instruments, equipped with a phase extender apparatus and a Q-box module was used.<sup>[17]</sup> Etched-silicon probes (pyramidal-shape tip, nominal curvature 10 nm, nominal internal angle 35°) were used. During the scanning, the 125- $\mu\text{m}$ -long cantilever, with a nominal spring constant in the range of 20–100 N/m, oscillated at its resonance frequency (~330 kHz). Height and phase images were collected by capturing 512 × 512 points in each scan and the scan rate was maintained below 1 line per second. During the imaging the temperature and humidity were about 25 °C and 40%, respectively.

## Supporting Information

Supporting Information is available from the Wiley Online Library or from the author.

## Acknowledgements

L.C. thanks the EPSRC for funding and the Royal-Society Wolfson Foundation for a Merit Award, and the University of Glasgow. B.P. acknowledges Italian MiUR (FIRB Futuro in Ricerca 2008, Laboratorio Pubblico-Privato PLAST\_ICs), MiUR (PON R&C 2007-2013, "Ambition Power - PON01\_00700") and the University of Palermo for funding. A correction was made to Ligand L1 of Table 1 on July 8, 2013.

- [1] a) D.-L. Long, E. Burkholder, L. Cronin, *Chem. Soc. Rev.* **2007**, *36*, 105–121; b) M. T. Pope, A. Müller, *Angew. Chem. Int. Ed. Engl.* **1991**, *30*, 34–48.
- [2] a) D.-L. Long, R. Tsunashima, L. Cronin, *Angew. Chem.* **2010**, *122*, 1780–1803; *Angew. Chem. Int. Ed.* **2010**, *49*, 1736–1758; b) C. L. Hill, *Chem. Rev.* **1998**, *98*, 1–2; c) C. Musumeci, M. H. Rosnes, F. Giannazzo, M. D. Symes, L. Cronin, B. Pignataro, *ACS Nano* **2011**, *5*, 9992–9999.
- [3] a) J. S. Anderson, *Nature* **1937**, *140*, 850; b) H. T. Evans, *Acta Cryst. B* **1974**, *30*, 2095–2112.
- [4] B. Hasenknopf, R. Delmont, P. Herson, P. Gouzerh, *Eur. J. Inorg. Chem.* **2002**, 1081–1087.
- [5] a) Y.-F. Song, N. McMillan, D.-L. Long, S. Kane, J. Malm, M. O. Riehle, C. P. Pradeep, N. Gadegaard, L. Cronin, *J. Am. Chem. Soc.* **2009**, *131*, 1340–1341; b) Y.-F. Song, N. McMillan, D.-L. Long, J. Thiel, Y. L. Ding, H. S. Chen, N. Gadegaard, L. Cronin, *Chem.-Eur. J.* **2008**, *14*, 2349–2354; c) J. Thiel, D. Yang, M. H. Rosnes, X. Liu, C. Yvon, S. E. Kelly, Y.-F. Song, D.-L. Long, L. Cronin, *Angew. Chem.* **2011**, *123*, 9033–9037; *Angew. Chem. Int. Ed.* **2011**, *50*, 8871–8875; d) C. Allain, S. Favette, L. M. Chamoreau, J. Vaissermann, L. Ruhlmann, B. Hasenknopf, *Eur. J. Inorg. Chem.* **2008**, 3433–3441; e) Y.-F. Song, D.-L. Long, L. Cronin, *Angew. Chem.* **2007**, *119*, 3974–3978; *Angew. Chem. Int. Ed.* **2007**, *46*, 3900–3904; f) P. R. Marcoux, B. Hasenknopf, J. Vaissermann, P. Gouzerh, *Eur. J. Inorg. Chem.* **2003**, 2406–2412; g) S. Favette, B. Hasenknopf, J. Vaissermann, P. Gouzerh, C. Roux, *Chem. Commun.* **2003**, 2664–2665.
- [6] a) M. H. Rosnes, C. Musumeci, C. P. Pradeep, J. S. Mathieson, D.-L. Long, Y.-F. Song, B. Pignataro, R. Cogdell, L. Cronin, *J. Am. Chem. Soc.* **2010**, *132*, 15490–15492; b) Y.-F. Song, D.-L. Long, S. E. Kelly, L. Cronin, *Inorg. Chem.* **2008**, *47*, 9137–9139.
- [7] C. Musumeci, A. Luzio, C. P. Pradeep, H. N. Miras, M. H. Rosnes, Y.-F. Song, D.-L. Long, L. Cronin, B. Pignataro, *J. Phys. Chem. C.* **2011**, *115*, 4446–4455.
- [8] B. Pignataro, *J. Mater. Chem.* **2009**, *19*, 3338–3350.
- [9] E. A. P. Ginsberg, *Inorg. Syn.* **1990**, *27*, 78–79.
- [10] a) E. A. Meyer, R. K. Castellano, F. Diederich, *Angew. Chem. Int. Ed.* **2003**, *42*, 1210–1250; b) I. G. Dance, in *The Crystal as a Supramolecular Entity* (Ed: G. R. Desiraju), John Wiley and Sons, Inc., New York **1996**, pp.137–233; c) C. A. Hunter, K. R. Lawson, J. Perkins, C. J. Urch, *J. Chem. Soc., Perkin Trans.* **2001**, *2*, 651–669; d) I. Dance, in *Encyclopedia of Supramolecular Chemistry*, 2-volume set (Eds: J. L. Atwood, J. W. Steed), Taylor and Francis, Boca Raton, USA **2004**, pp.1077–1093.
- [11] a) A. G. Orpen, L. Brammer, F. H. Allen, O. Kennard, D. G. Watson, R. Taylor, *J. Chem. Soc., Dalton Trans.* **1989**, S1–S60; b) I. Dance, *CrystEngComm* **2003**, *5*, 208–221; c) G. A. Jeffrey, *An Introduction to hydrogen bonding (Topics in Physical Chemistry)* (Ed: D. G. Truhlar), Oxford University Press, New York **1997**.
- [12] T. Ito, K. Sawada, T. Yamase, *Chem. Lett.* **2003**, *32*, 938–939.
- [13] B. Pignataro, L. Sardone, G. Marletta, *Langmuir* **2003**, *19*, 5912–5917.
- [14] A. Raudino, B. Pignataro, *J. Phys. Chem. B* **2007**, *111*, 9189–9192.
- [15] T. Ito, H. Yashiro, T. Yamase, *Langmuir* **2006**, *22*, 2806–2810.
- [16] H. S. Rho, H. S. Baek, D. H. Kim, I. S. Chang, *Bull. Korean Chem. Soc.* **2006**, *27*, 584–586.
- [17] B. Pignataro, L. Chi, S. Gao, B. Anczykowski, C. Niemeyer, M. Adler, H. Fuchs, *Appl. Phys. A* **2002**, *74*, 447–452.

Received: October 11, 2012  
Revised: December 6, 2012  
Published online: February 7, 2013